Flow transition of a low Prandtl number fluid in an inclined three-dimensional cavity

Rafael Delgado-Buscalioni, Emilia Crespo del Arco, Patrick Bontoux

▶ **To cite this version:**

Rafael Delgado-Buscalioni, Emilia Crespo del Arco, Patrick Bontoux. Flow transition of a low Prandtl number fluid in an inclined three-dimensional cavity. European Journal of Mechanics - B/Fluids, 2001, 20 (5), pp.657-672. 10.1016/S0997-7546(01)01140-2 . hal-00835759

HAL Id: hal-00835759
https://hal.science/hal-00835759

Submitted on 10 May 2024

HAL is a multi-disciplinary open access archive for the deposit and dissemination of scientific research documents, whether they are published or not. The documents may come from teaching and research institutions in France or abroad, or from public or private research centers.

L'archive ouverte pluridisciplinaire **HAL**, est destinée au dépôt et à la diffusion de documents scientifiques de niveau recherche, publiés ou non, émanant des établissements d'enseignement et de recherche français ou étrangers, des laboratoires publics ou privés.

Distributed under a Creative Commons Attribution - NonCommercial - NoDerivatives 4.0 International License

Flow transitions of a low-Prandtl-number fluid in an inclined 3D cavity

Rafael Delgado-Buscalioni [a], Emilia Crespo del Arco [a], Patrick Bontoux [b]

[a] *Depto. Física Fundamental, UNED, Aptdo. 60141, Madrid, Spain*
[b] *LMSNM, CNRS, IMT Château Gombert, 38 Frédéric Joliot Curie, Marseille, France*

(Received 3 March 2000; revised 1 November 2000; accepted 28 March 2001)

Abstract – We present a numerical and theoretical investigation on the natural convection of a low Prandtl number fluid (Pr = 0.025) in 2D and 3D side-heated enclosures tilted α = 80◦ with respect to the vertical position. The choice of this inclination angle comes from a previous linear stability analysis of the basic (plane-parallel) flow that predicts the same critical Ra for longitudinal oscillatory and stationary transversal modes. In both the 2D and 3D enclosures the first transition gradually leads to a transversal stationary centered shear roll. In the 2D geometry the flow becomes time-dependent and multicellular (3 rolls) at the onset of a Hopf bifurcation, followed by subsequent period-doubling. On the other hand, in the 3D enclosure, the onset of oscillations is due to a fully three-dimensional standing wave composed of three counter-rotating longitudinal rolls. The further evolution of the 3D flow qualitatively agrees with previous experiments (J. Crystal Growth, 102 (1990) pp. 54–68): a quasiperiodic flow followed by a frequency locked state. The main contribution of this work is the analysis of the flow structure underlying the secondary frequency: a transversal wave composed of two shear rolls that coexist with the three longitudinal cells. This is the first numerical work that explicitly illustrates this scenario which was suggested at the onset of the biperiodic regime in many of the previous experiments.

inclined Hadley configuration / instabilities / oscillations / bifurcation / numerical calculation

Nomenclature

A_z, A_y	aspect ratios: H/L, H/D
g	acceleration due to gravity
f_1, f_2	fundamental frequency and secondary frequency
$f_1^{(2D)}$	fundamental frequency for the 2D calculations
Gr	Grashof number, $g\beta\Delta T\, h^4/L\nu^2$
H, D, L	dimensions of the enclosure in the x, y and z direction
h,d	semi-depth and semi-width of the enclosure, $h = H/2$, $d = D/2$
K	nondimensional axial temperature gradient at the core
m	wavenumber along the y direction
Pr	Prandtl number, ν/κ
Ra	Rayleigh number, $g\beta\Delta T\, h^4/L\nu\kappa$

* Correspondence and reprints.
E-mail address: rafa@fisfun.uned.es (R. Delgado-Buscalioni).

T	nondimensional temperature
ΔT	dimensional temperature difference between the end-walls
δt	time step
$\mathbf{v} = (u, v, w)$	nondimensional velocity (along x, y and z directions)

Greek symbols

α	inclination of the z axis with respect to the vertical direction
β	coefficient of thermal expansion
κ	thermal diffusivity
ν	kinematic viscosity
ρ	fluid density

1. Introduction

Since the invention of the Bridgman technique for the production of homogeneous pure semiconductor crystals, there has been a considerable interest in the flow of liquid metals in shallow cavities with externally imposed horizontal temperature gradients. Using the Bridgman technique in horizontal cavities it was noticed that above a certain temperature gradient, undesirable striations of solute were found in the crystal. The early experiments (see Hurle et al. [1] and references therein) showed that the striations were due to temperature oscillations, induced by time-dependent flow, that cause the crystal to consecutively solidify and remelt at the interface. Subsequent experimental and theoretical studies were devoted to the stability of the steady regime of this type of flow, known as Hadley circulation. A great variety of instabilities were revealed and soon the Hadley configuration was also thought of as a practical support for investigating the routes to chaos.

The steady basic flow is essentially bidimensional and flows in the section (x, z) of *figure 1*. For a small enough temperature gradient it consists of a steady motion that flows upwards in the hot region, downwards in the cold region and traverses the core of the enclosure as a parallel flow, when far enough from the end walls. In the inclined configuration the torque created by buoyancy depends also on the cross-stream temperature differences and for $\alpha < 90°$ its effect is to enhance the convection. This fact motivated some studies of the basic unicellular flow in the inclined configuration that showed that by a suitable choice of the inclination angle,

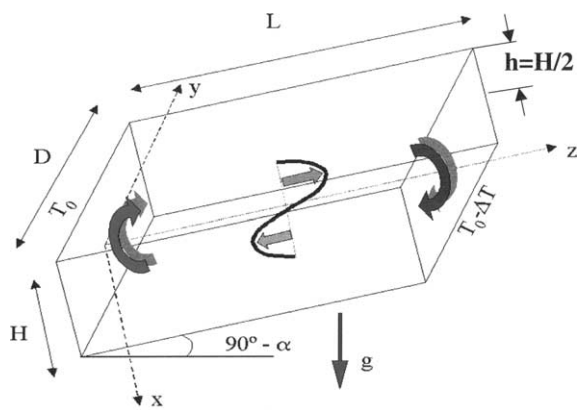

Figure 1. Geometry of the problem and sketch of the basic flow.

larger transport rates can be obtained [2,3]. Stability analyses of the basic flow in the inclined configuration may be found in [4–6]. The presence of a component of the buoyancy force along the heating axis of the enclosure enables several instability mechanisms, which arise due to momentum-temperature couplings that are not possible in the horizontal configuration. Furthermore, the inclined geometry makes more accessible the investigation of interactions between different types of instabilities.

In any case, most of the previous investigations on this type of flow considered horizontal cavities (see [7–9] for recent reviews). The stability of the basic Hadley circulation to transversal and longitudinal disturbances was first studied by Hart (see [10,11] and references therein) for infinite long cavities (the parallel flow solution). His results were then revised by Kuo and Korpela [12] and Laure [13]. Concerning low-Prandtl-fluids they showed that for $Pr > 0.034$ the Hadley cell breaks down because of the oscillatory longitudinal instability, whereas for lower Prandtl number, stationary transversal shear disturbances are the most dangerous. Theoretical explanations for the physical origin of the oscillatory longitudinal instability and analytical trends for its frequency were given by Hart [10,11] and Gill [14]. After the pioneering experimental works [1], several experiments investigated the evolution of the flow with increasing values of the control parameter. Hung and Andereck [15] used mercury in a wide and long enclosure ($H \times D \times L = 1 \times 17.78 \times 17.89$), Pratte and Hart [16,17] used the same fluid ($Pr \simeq 0.026$) and cavities with several aspect ratios. Braunsfurth and Mullin [8] used a $1 \times 1.35 \times 4$ enclosure and could change the value of the Prandtl number of their working fluid (liquid gallium) by changing the mean temperature of the enclosure. Recently Davoust et al. [18] used mercury in a cylindric geometry with a small diameter-to-length aspect ratio ($1/10$). The experiments showed that once the oscillatory regime associated to the longitudinal instability is established, the next bifurcation leads to a biperiodic flow with a (usually lower) secondary frequency. From a dynamical point of view, the details of the secondary transition depends on the geometry, the aspect ratio and the Prandtl number and was characterized by either a period doubling transition [17], a subharmonic cascade [19] or by a quasiperiodic flow [8,15,16] followed in some cases by frequency-locked states [16]. Some previous experimental works have been focused in the characterization of different types of bifurcations, using the time signals of the flow (see [8,20]). In these works there was a considerable interest in finding regions of the space of parameters where two different type of bifurcations intersects. For instance, Braunsfurth and Mullin [8] explored a region of the $Pr-Gr$ space and found several quasiperiodic states that arise at values of the parameter space near the intersection of two lines of Hopf bifurcations. Also, the codimension of the problem may be increased by introducing a magnetic field perpendicular to the plane of the basic flow, whose intensity is determined by Hartman number (see the experiments in refs. [18,20]). By using this procedure McKell et al. [20] characterized several routes to chaos from secondary Hopf bifurcations and period-doubling bifurcations.

However, the flow structure at the emergence of the secondary frequency is not so well studied. The inherent limitations of the experiments were explained by Hung and Andereck [15] (see also [16]). When working with liquid metals, the most sensitive way to capture the flow structure consists on placing thermistor probes from point to point across the surface of the enclosure. The deviation in the temperature field produced by the transverse rolls is extremely small and hence unobservable with the thermistor sensor. As a consequence the experiments are limited to follow the temperature variations induced by the longitudinal modes. Although it is therefore very difficult to elucidate what kind of motion is related to the secondary frequency from the experimental outcome (see the method proposed in [16], which measures the phase lag between the probes), interesting enough is that all those experimental investigations that tried to understand the connection between the dynamics and the spatial structure of the flow [15,16,18], suggested that the novel structure underlying the onset secondary frequency could be a transversal wave composed by shear rolls which coexist, as Ra is increased, with the longitudinal one.

On the other hand, the description of a fully developed 3D biperiodic flow in a confined geometry has rather large overheads for a purely theoretical analysis. Previous theoretical approaches were able to give trends for the fundamental frequency [10,11] or to perform a weakly non-linear analysis of the interactions between modes in an unbounded geometry, valid in the neighbourhood of the secondary bifurcation (see e.g., [21]). In view of these facts, numerical studies are specially needed to observe the detailed flow structure of these low-Prandtl fluids at pre-chaotic stages. A large part of the numerical calculations on the horizontal configuration were made using two-dimensional geometry (see [7] for a review). Although a good agreement was found between them, any investigation in 2D is restricted to transversal instabilities. In 2D enclosures at low Prandtl number, the flow becomes oscillatory after the onset of stationary shear rolls and it gains in complexity by several possible paths (see [22,23]), which as a matter of fact, do not satisfactory explain the flow oscillations found in the previous experiments. Demands for numerical calculations for the three-dimensional flow were made [15,16]. In particular, one of the cases considered by Pratte and Hart [16] (a $Pr = 0.026$ fluid in a $1 \times 2 \times 4$ enclosure) has been numerically studied by several authors [24,9]. Henry and Buffat [9] estimated the critical Grashof number by assuming a Hopf bifurcation and extrapolating to zero oscillation amplitude. They reported a critical Rayleigh number of $Ra = 54.8 \pm 0.5$ and a frequency of $f_1 = 13.6\nu/H^2$, while the biggest discrepancy previously reported (experimental result) is $Ra = 68.74$ and 14.3 (see [9] for a detailed comparison). Nevertheless, in these numerical studies, the flow structure at the onset of the secondary frequency was not considered. Another fact is that in the $1 \times 2 \times 4$ enclosure selected by the previous numerical calculations [24,9] the transversal and longitudinal instabilities appear respectively as one shear roll in the plane of the basic flow ((x, z) in *figure 1*) and one longitudinal roll in the perpendicular plane (x, y). As noted by Braunsfurth et al. [7] multicellular flows have not yet been reported in three-dimensional numerical results. This lack of numerical studies was also mentioned by Henry and Buffat [9] who expressed the interest of investigating other aspect ratios.

In this paper we present numerical calculations of the natural convection of a fluid with $Pr = 0.025$ in a 2D ($H \times L = 1 \times 4$) enclosure and a 3D one with dimensions $1 \times 6 \times 4$. Both are inclined at $\alpha = 80°$ with respect to the vertical position and heated along the side of length $L = 4H$. In principle, this set of parameters was chosen to promote the interaction between longitudinal and transversal multicellular modes. First, the selection of the angle comes from a previous stability analysis [6], which indicated that for a $Pr = 0.025$ fluid the codimension-two line for the transversal and longitudinal instabilities passes through $\alpha = 80°$. Second, the selected width ($D = 6H$) is larger than that considered in the previous 3D numerical calculations [24,9] ($D = 2H$) and this fact enables the development of a longitudinal standing wave with multicellular structure (three counter-rotating rolls) along the (x, y) plane. The resulting flow, at the largest Ra considered, has two leading frequencies and consists of a longitudinal wave that coexists with two co-rotating transversal cells. The relevant outcome of this result is the possibility of relating the spatial structure of the flow with its temporal behaviour at the onset of bi-periodicity.

The rest of the paper continues as follows. Section 2 presents the governing equations. The results concerning the flow in the 2D geometry are presented in section 3. The bulk of the paper, in section 4, deals with the flow in the 3D enclosure and focuses its attention on the relation between the dynamical behaviour and flow structure at the subsequent transitions. Conclusions are given in section 5.

2. Equations of motion

Let us consider the flow in the enclosure of *figure 1*. The dimensions of the enclosure along x, y and z directions are respectively $H = 2h$, D and L. The z-axis is inclined an angle $180° - \alpha$ with respect to the gravity vector, $\mathbf{g}$ and an excess of temperature ΔT is imposed between the walls separated by L. The

enclosure is filled with an incompressible fluid with thermal expansion coefficient β, kinematic viscosity ν, and thermal diffusivity κ. For any non-vertical position $\alpha \neq \{0°, 180°\}$ mechanical equilibrium is impossible and a convective motion is established. We assume that the flow is governed by the Navier–Stokes and heat transport equations with the Boussinesq approximation. By using, h^2/ν, h, ν/h, ΔT and $\rho_0 \nu^2/h^2$ respectively as scales for time, length, velocity, temperature and pressure the nondimensional equations are (1)–(3)

$$\nabla \cdot \mathbf{v} = 0, \tag{1}$$

$$\left(\frac{\partial \mathbf{v}}{\partial t} + \mathbf{v} \cdot \nabla \mathbf{v}\right) = -\nabla P + \nabla^2 \mathbf{v} - 2Ra\, Pr^{-1} A_z^{-1}\, T\, \mathbf{e}_g, \tag{2}$$

$$\frac{\partial T}{\partial t} + (\mathbf{v} \cdot \nabla) T = Pr^{-1} \nabla^2 T. \tag{3}$$

The walls are rigid (no-slip condition is assumed) and the heat flux perpendicular to the walls is zero (insulating walls). These conditions, along with the temperature at the end walls, yields the following boundary conditions,

$$\mathbf{v} = 0 \quad \text{at } x = \pm 1,\ y = \pm A_y^{-1},\ z = \{0, 2A_z^{-1}\}, \tag{4}$$

$$T = 0 \quad \text{at } z = 0; \qquad T = -1 \quad \text{at } z = 2A_z^{-1}, \tag{5}$$

$$\frac{\partial T}{\partial x} = 0 \quad \text{at } x = \pm 1, \tag{6}$$

$$\frac{\partial T}{\partial y} = 0 \quad \text{at } y = \pm A_y^{-1}, \tag{7}$$

$$\tag{8}$$

where $\mathbf{e}_g = \sin\alpha\, \hat{\mathbf{i}} - \cos\alpha\, \hat{\mathbf{k}}$, is the gravity vector and $\mathbf{v}$, T, and p the dimensionless velocity, temperature, and pressure. The Rayleigh number and Prandtl number are defined respectively as $Ra = g\beta\Delta T h^4/L\nu\kappa$ and $Pr = \nu/\kappa$.

3. Two-dimensional flow

3.1. Numerical method

By taking the curl in the Navier–Stokes equation an equation for the vorticity ($-\nabla \times \mathbf{v}$) is obtained. For the two dimensional flow in the (x, z)-plane the vorticity is parallel to the y-direction and therefore may be treated as an scalar quantity. Also, a stream-function can be defined in such a way that the Laplacian of the stream-function equals the vorticity. A Chebyshev-collocation pseudospectral method has been used for solving the unsteady vorticity and heat equations in vorticity-stream function variables for the closed two-dimensional geometry (i.e. for the (x, z)-plane). The spatial approximation in both directions is done by expanding the flow variables in truncated series of Chebyshev polynomials [25]. The time discretization is obtained through an Adam-Bashforth, second order Backward Euler scheme [25]. This is a semi-implicit finite difference scheme; i.e., the diffusive terms are treated implicitly while the non-linear terms are treated explicitly. The equations for the stream function and vorticity consist of a Stokes-type problem which is solved by using the Influence Matrix technique [25].

In all the studied cases a grid of 31×81 collocation points were enough to obtain accuracies of better than about 2%. The smallest time steps were $\delta t = 10^{-4} h^2/\nu$ and correspond to calculations for Ra above the Hopf bifurcation. We refer to [22] for a detailed study on the grid and time step solution's dependence in a case

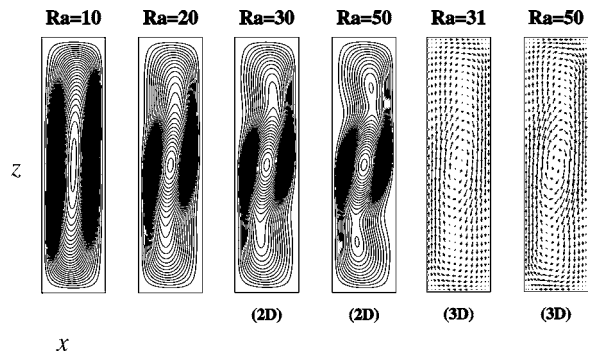

Figure 2. From left to right, the first three figures correspond to the streamfunction of the 2D stationary flow. The vector field plots correspond to the 3D oscillatory flow at $Ra = 30$ and $Ra = 47$ at approximately the center of the enclosure ($y = 0.05$).

($\alpha = 90°$, $H/L = 1/4$ and $Pr = 0$ and 0.015) very similar to that considered in this work. In [22] the typical meshes were 20×60 and similar time steps were used.

3.2. Results

The critical Rayleigh number for the onset of stationary transversal rolls obtained from the stability analysis of the strictly plane-parallel flow (valid for cavities with $L \gg H$) is $Ra = 13$ (see [6]). In the finite enclosure the distortion of the basic parallel flow begins to be observed at $Ra > 15$. As may be seen in *figure 2*, this distortion consists of a stationary shear roll that gradually grows at the center of the enclosure and detaches from the end walls as the Rayleigh number is increased. This gradual transition is an example of imperfect bifurcation induced by the presence of the end walls similar to those reported for $Pr = 0$ fluids in the horizontal enclosure with $A_z = 1/4$ [22,7] and in longer inclined cavities with $Pr \simeq 1$ [6]. At $55 < Ra \leqslant 60$ a transition to oscillatory flow occurs. Snapshots of the flow along a period are shown in *figure 3(a)*. In horizontal cavities ($\alpha = 90°$) and for lower Prandtl number ($Pr \leqslant 0.015$) a similar transition was reported and characterized as a Hopf bifurcation [22,26,27]. The snapshots shown in *figure 3(a)* are very similar to those presented by Pulicani et al. [22] for $Pr = 0.015$ and $\alpha = 90°$, who found the Hopf bifurcation at $Gr = 2375$. For the same parameters ($A_z = 1/4$ and $Pr = 0.015$) Skeldon et al. [23] calculated the dependence of the critical Grashof number for the onset of oscillations with the inclination angle showing that it has a minimum value around $\alpha \sim 50°$ ($Gr \simeq 1350$) while for $\alpha = 80°$ it is around $Gr \simeq 1950$. Nevertheless, as shown also in [23], in the horizontal enclosure, the critical Grashof number for the onset of oscillations increases rapidly with Pr (e.g., $Gr = 6231.25$ for $Pr = 0.021$) and for $Pr = 0.025$ no evidence of oscillations were found for Grashof numbers up to 9375. Interestingly enough is that for $\alpha = 80°$ and $Pr = 0.025$ we observed oscillations at a much lower Grashof number, $Gr = 2400$. Similar abrupt changes between the inclined and the horizontal configurations were also observed in the onset of transversal instabilities as the value of Pr was increased ([6,4]). These differences could be explained by considering the energy balance of the critical modes ([6]). Briefly, as Pr increases, the thermal effects become increasingly important and if the enclosure is inclined and heated-from-below ($\alpha < 90°$) the transversal perturbation can obtain a increasing part of kinetic energy by a destabilizing mechanism that couples the cross-stream advection of heat and the z-component of the buoyancy force.

As shown in *figure 3(a)*, the first Hopf bifurcation does not break the centro-symmetry of the flow. This symmetry is preserved until $Ra < 90$, but for $Ra \geqslant 100$ a period-doubling transition is observed and at any instant the centro-symmetry is broken. Snapshots of the flow at $Ra = 100$ and along a period of the fundamental frequency $1/f_1^{(2D)}$ are shown in *figure 3(b)*. Note that after the period-doubling transition the flow

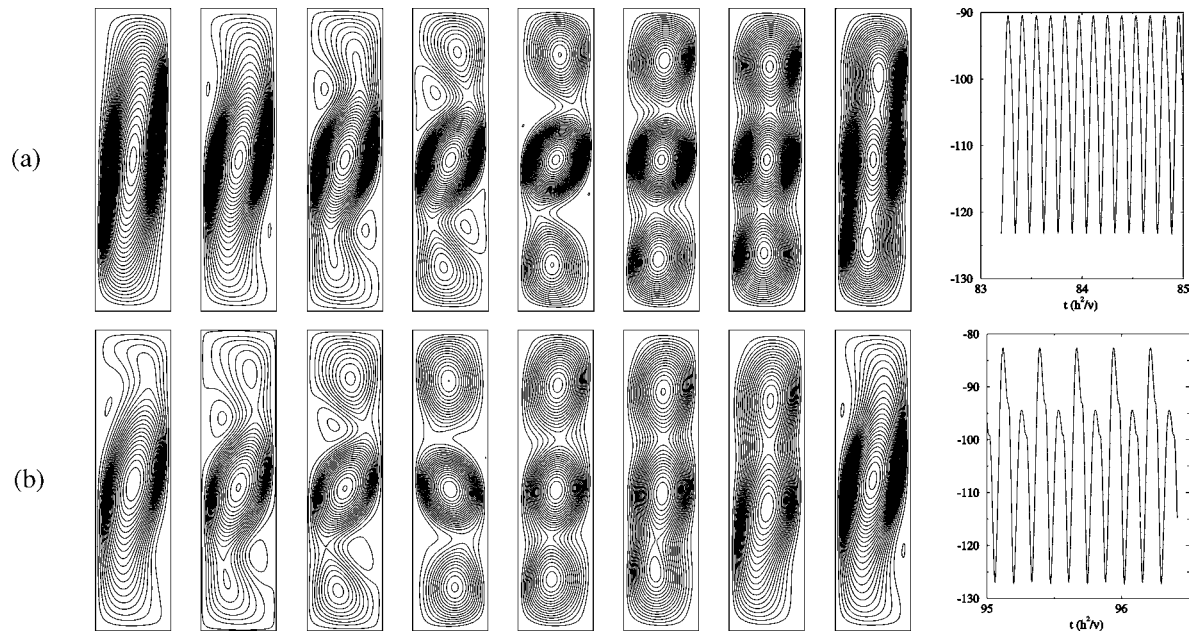

Figure 3. Streamfunctions of the two-dimensional flow: (a) Snapshots along a period of motion at $Ra = 90$ and (b) at $Ra = 100$ along the period associated to the fundamental frequency, $1/f_1^{(2D)}$. The time signal of the streamfunction at $x = 0.12$ and the central section $z = A_z^{-1}$ is shown in both cases.

preserves the centro-symmetry between states separated by a period of the fundamental frequency (which is the semiperiod of the oscillation, as long as the flow is periodic in $2/f_1^{(2D)}$). As may be seen in *figure 7(c)*, the fundamental frequency grows with Ra approximately as the maximum z-velocity of the mean flow ($\langle w_{\max}\rangle \simeq 0.31 Ra^{4/7} Pr^{-1}$). A fluid particle needs a time of about $(\langle w_{\max}\rangle A_z/4)^{-1}(h^2/\nu) \simeq (0.75\, Ra^{4/7})^{-1} h^2/\nu$ to cross the enclosure along z-direction and return to the starting point. The fundamental frequency increases as $0.53\, Ra^{4/7}\nu/h^2$. This indicates that the origin of the oscillation of the shear rolls is the convection of the mean flow along the z-axis. Spectra with both $f_1^{(2D)}$ and $f_1^{(2D)}/2$ are observed at least for $100 \leqslant Ra \leqslant 190$. Although we did not advance further in the control parameter, it is probable that at large enough Ra a steady branch with two co-rotating shear rolls coexists with the oscillatory solution. The existence of a bicellular solution was reported in fluids with $Pr = 0$ and $Pr = 0.015$ (with conducting walls) in the work of Pulicani et al. [22]. Also Winters [26] predicts that the bicell is the most stable solution at large Gr. Nevertheless, in the case of insulating boundaries and larger Prandtl number ($Pr = 0.025$), the onset of the bi-cell flow is shifted towards higher values of Ra because of the relatively stronger damping caused by the stably stratified core (for instance, in [22] the bicell was not reported for $Pr = 0.015$ and insulating walls).

4. Three-dimensional flow

4.1. Numerical aspects

Using the same values of the Prandtl number and the inclination ($Pr = 0.025$ and $\alpha = 80°$) we carried out numerical simulations of the flow in a 3D enclosure with the same H/L aspect ratio (1/4) and $A_y = H/D = 1/6$. We have used a commercial code [1] that solves the coupled mass, momentum and energy conservation

[1] CFD2000 by Adaptive Research, Pacific Sierra Corp., 1997.

Table I. Comparison of several flow quantities obtained for $Ra = 93.75$ and several meshes and time steps, δt. $\langle u_{\max}\rangle_t$ is the time averaged maximum value of u and $A_w^{(y)}$ is the maximum amplitude of the spatial variation of w along y-direction measured in the core of the enclosure ($L/4 < z < 3L/4$). The fundamental frequency scaled with ν/h^2 is f_1. In all cases the flow is oscillatory.

Mesh	δt	$\langle u_{\max}\rangle_t$	$\langle v_{\max}\rangle_t$	$\langle w_{\max}\rangle_t$	$A_w^{(y)}$	$A_T^{(y)}$	f_1
$15 \times 46 \times 35$	0.002	93.03	83.75	163.64	37.43	0.170	4.464
$15 \times 46 \times 35$	0.001	93.70	83.10	164.02	37.52	0.172	4.481
$15 \times 46 \times 71$	0.002	95.52	85.74	169.73	39.03	0.177	4.465
$15 \times 91 \times 35$	0.002	96.89	85.90	170.10	39.72	0.175	4.470

Table II. Results for $Pr = 0.025$, $\alpha = 80^\circ$ and $A_z = 1/4$, $A_y = 1/6$. The notation is as follows: BF, basic stationary flow; S, stationary flow; P1, oscillatory flow; QP, quasiperiodic flow; P2, periodic flow with two locked frequencies. The fundamental frequency, f_1, and the secondary one, f_2, are given in ν/h^2. Results have been obtained with the $16 \times 46 \times 36$ mesh and a time step $\delta t = 0.002h^2/\nu$.

Ra	$R = K\,Ra$	Dynamics	f_1	f_2	n° long. cells	n° trans. cells
$\leqslant 15$	$\leqslant 15$	BF	–	–	0	0
31.25	28.56	S	–	–	0	1
46.875	40.5	P1	3.27	–	3	1
62.5	50.44	P1	3.65	–	3	1
93.75	68.81	P1	4.47	–	3	1
156.25	93.29	P1	5.49	–	3	1
195.31	116.21	QP	6.07	1.135	3	2
218.75	118.87	P2	6.35	1.155 ($2f_1/11$)	3	2

equations (equations (1)–(3)) by a finite volume method. The coupling between velocity and pressure is solved by a PISO algorithm. For a detailed explanation of the numerical method see [28].

In order to check out the grid dependency of the solution, a mesh refinement was made in several cases which presented both oscillatory and stationary behaviour. In the oscillatory case the dependence with the time step was also studied. *Table I* compares the values of some flow quantities obtained with several grids in calculations made with $Ra = 93$ (an oscillatory case). Note that the maximum difference between the maximum mean velocities is about 4% indicating that the more coarse-grained mesh retains the main characteristic of the flow. A precise representation of the oscillatory solutions has been guaranteed by using time steps of about $10^{-3}h^2/\nu$ which yield about 100 time steps per period. In any case, once the longitudinal wave is established we found an upper boundary for the time step that preserves the stability of the numerical algorithm: for time steps greater than $\delta t > 0.002\,h^2/\nu$, it lead either to a non-oscillatory behaviour or to the divergence of the solution (for $\delta t > 0.005$). In order to physically understand this fact, note that the fluid takes a time of order $h/\langle u_{\max}\rangle \sim 0.01h^2/\nu$ to cross the shorter direction of the enclosure (see *table I*). This clearly implies an upper threshold for δt, so that to properly reproduce the oscillatory flow, one needs several evaluations of the flow on its motion along the shorter direction. Concerning the length of the transients, in those calculations where the longitudinal was present, the transient time varied between 5 and $7h^2/\nu$. These values are of the same order as the characteristic diffusion time of the wave along the longest direction of the enclosure (y): $(d^2/(\nu\kappa)^{1/2} \simeq 6h^2/\nu)$. Both facts (the limit for δt and the long transient times) impose large computational times (for instance for the finer mesh ($15 \times 91 \times 35$), 5 hours per cycle in an 400 MHz machine).

4.2. Results

Table II shows the main characteristics of the flow obtained from our numerical calculations as the Rayleigh number were increased. In particular, we show the value of the local Rayleigh at the core, $R = K\,Ra$ (note that

it is calculated with the local temperature gradient along z direction, $-K\Delta T/L$), the dynamical behaviour of the flow, the values of the fundamental and secondary frequencies, f_1 and f_2, and the number of longitudinal and transversal cells found in the core of the enclosure. In the following discussion, reference to *table II* shall be useful.

4.2.1. Gradual development of a stationary shear roll, $Ra \geqslant 20$

For $Ra \leqslant 47$, the flow remains stable to the longitudinal instability and it is essentially two-dimensional. Therefore, the comments made in a previous section for the 2D flow remain valid at this stage of the 3D flow. In particular, for $Ra \geqslant 20$, a transversal shear roll may be observed at the center of the (x, z)-plane and its amplitude gradually increases with Ra. *Figure 2* shows the similarity between the 2D flow and the 3D flow at the central (x, z)-plane ($y \simeq 0$) for $Ra = 30$ and $Ra = 50$.

4.2.2. The longitudinal oscillatory rolls, $Ra \geqslant 47$

The two-dimensional stationary flow is broken at $31.25 < Ra \leqslant 47$ due to the onset of an oscillatory flow with three longitudinal (counter-rotating) rolls along the y direction, which may be seen in *figure 4* for a slightly greater value of Ra. For the lowest value of Ra at which we observed the longitudinal wave ($Ra = 47$), the value of the local Rayleigh number at the core is $R = K\,Ra = 40$, the wavelength is approximately $4H$ (wave number $m = 0.785$) and the frequency is $f_1 = 3.27\nu/h^2$. For these values of R, m the frequency predicted by the linear stability analysis is $f = 3.45\nu/h^2$, very close to the numerical result. This clearly indicates that the flow corresponds to the onset oscillatory longitudinal instability obtained in the linear stability of the basic plane-parallel flow [4].

Some questions may arise concerning the wavenumber selection in the confined geometry. The critical wavenumber predicted by the linear stability analysis is $m = 0.34$. This gives a critical wavelength (without considering the confinement) of about $9H$, which is is larger than the width of the enclosure ($D = 6H$). On the other hand, the numerical calculations of Henry and Buffat [9] show that the onset longitudinal standing wave consists of a Hopf bifurcation which breaks some symmetries of the mean flow. We have observed the same ruptures of symmetries: the symmetry about $y = 0$ $(x, y, z, u, v, w, T) \rightarrow (x, -y, z, u, -v, w, T)$ and the reflection $(x, y, z, u, v, w, T) \rightarrow (-x, y, 2A_z^{-1} - z, -u, v, -w, -1 - T)$. Note that the symmetry about $y = 0$ is broken only if an odd number of longitudinal rolls develops along the y direction. The selection of the three roll pattern (instead of a unique longitudinal cell) probably occurs because it minimizes the diffusion; also, at the value of Ra of the transition, its wavenumber may have a slightly faster growth rate, as suggested by the stability analysis.

Recall that for $Ra > 20$ a shear roll develops in the center of the (x, z)-plane. Once the oscillatory flow is established, the transversal cell is convected by the longitudinal standing wave. Along a period of the oscillation the center of the shear roll moves in a ellipse at each (x, z)-section; the amplitude of the ellipse is maxima at those values of y where the standing wave has a valley and minima where it has a node (for instance, at the center section, $y = 0$). If one observes the sections of the velocity field shown *figures 5* and *6*, it is seen that the position of the center of the shear roll describes a sinusoidal path along the y axis. Essentially, the motion of the center of the transversal cell coincides with the description made in [9] in an enclosure with the same depth-to-length ratio, $H/L = 1/4$, and a shorter y-direction ($D = 2H$) occupied by one longitudinal roll.

4.2.3. The fundamental frequency, f_1

At least for $47 \leqslant R \leqslant 156$ the flow is oscillatory and the power spectra of the time signal shows a fundamental frequency f_1 and its higher harmonics (see *figure 8*). As mentioned above, in this range of Ra, one shear roll coexists with the longitudinal wave but the dynamics of the oscillation is essentially governed by the

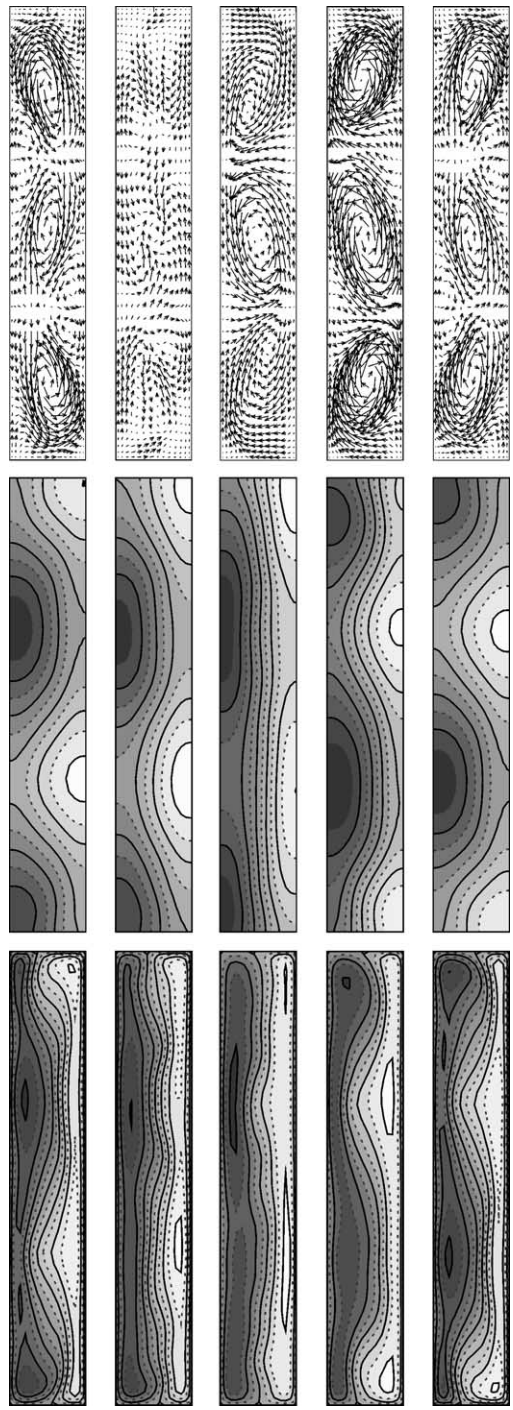

Figure 4. From above to below, snapshots of the vector field, isothermals and isovalues of the z-velocity at the plane $z = 1.1A_z^{-1}$ (near the center of the enclosure) along a semiperiod of the oscillation. The results correspond to $Ra = 62.5$ and the fundamental frequency is $f_1 = 3.65\nu/h^2$.

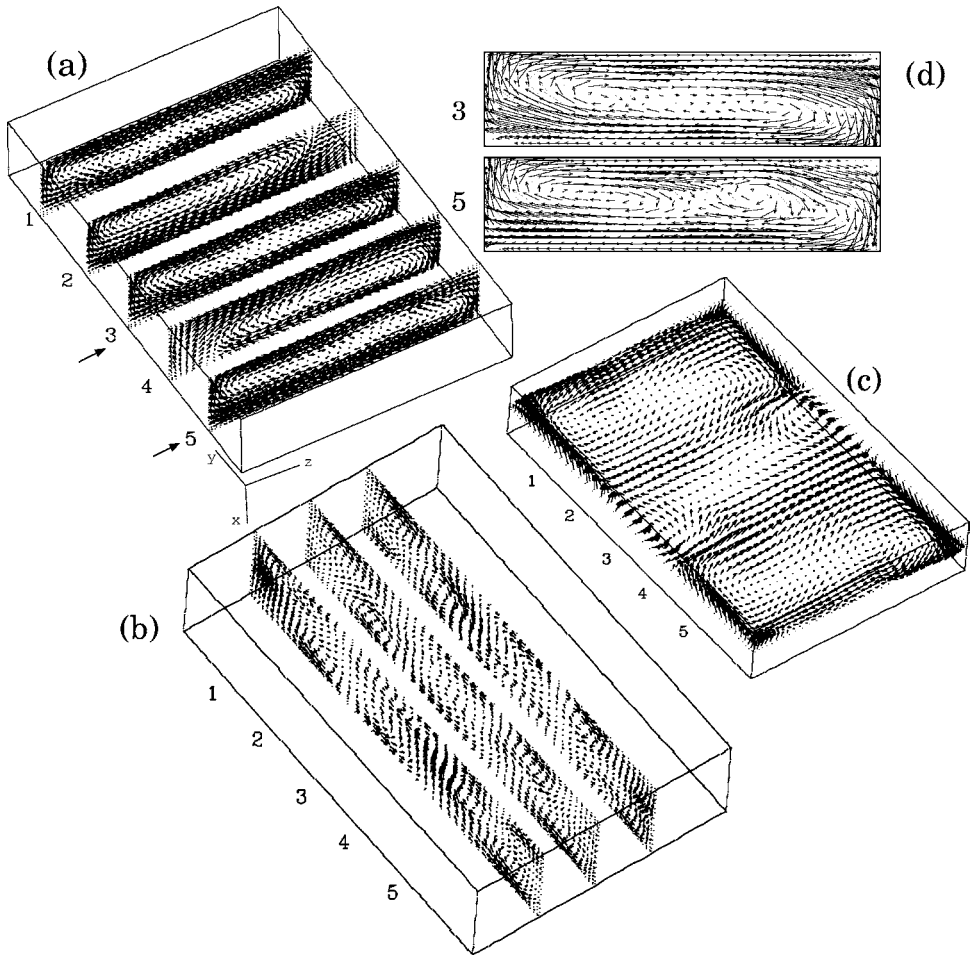

Figure 5. Snapshots of the flow at $Ra = 195$ at an instant of minimum intensity of the perturbative flow in the (x, y)-plane. (a), (b) and (c) show cuts of the vector field at respectively $y = cte$, $z = cte$ and $x = cte$ planes. (d) Magnification of the vector field in the $y = cte$ planes labeled in (a) by 3 and 5.

longitudinal wave. To show this fact, we shall compare the trend of the numerical calculated values of f_1 with a theoretical prediction for the frequency associated to the longitudinal wave, obtained by extrapolating to the inclined case the approximation made by Hart [10,11] for the horizontal enclosure

$$2\pi f_{\text{teor}} = \left(\frac{m^2 K\, Ra \sin(\alpha) \langle w' \rangle}{\pi^2 + m^2} \right)^{1/3} \nu / h^2, \tag{9}$$

where $\langle w' \rangle$ denotes the x derivative of the mean flow and K the temperature z-gradient at the core region Note that in equation (9) the nondimensional group associated to buoyancy is $K\, Ra \sin(\alpha)$, instead of Ra which appears in the relationship given in [10,11]. This means that we are implicitly assuming that: first, for the angle considered, the contribution of the z-component of the buoyancy force is negligible for the dynamics of the oscillation; and second, that the perturbative motion originates in the core of the enclosure and hence the proper relation has to be expressed in terms of the the local Rayleigh number at the core, $K\, Ra$. In order to evaluate the terms of equation (9) we have measured K by averaging in the core (between $L/4 < z < 3L/4$) the temperature z-gradient along one oscillation cycle. The maximum z-velocity of the mean flow, $\langle w_{\max} \rangle$ has

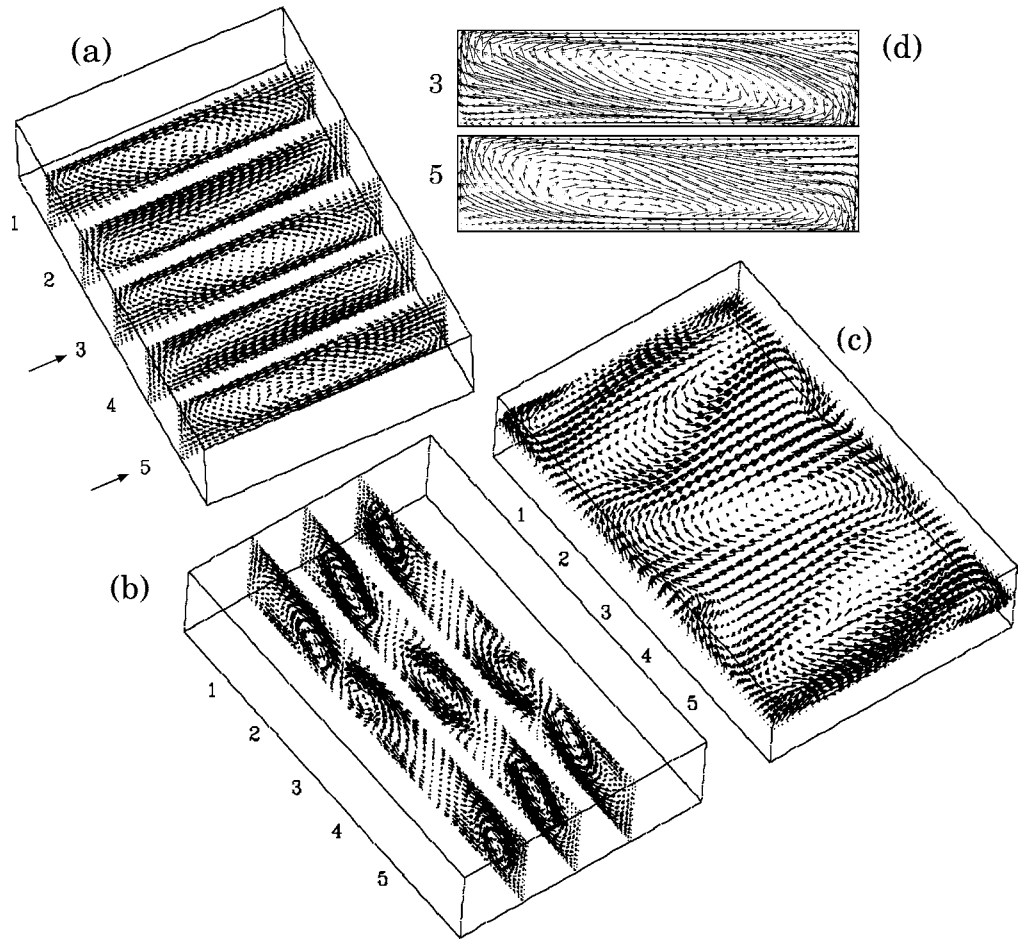

Figure 6. Snapshots of the flow at $Ra = 195$ at an instant of maximum intensity of the perturbative flow in the (x, y)-plane. The snapshots correspond to an instant of time separated from those in *figure 5* by a quarter of period of the fundamental cycle. For (a), (b), (c) and (d) see the caption of *figure 5*.

been also evaluated in this way. The mean velocity profile along the x direction is S-shaped and its maximum is located near $|x| = 1/2$, hence the relation $\langle w' \rangle \simeq 2\langle w_{\max} \rangle$ is approximately satisfied. *Figures 7(b)* and *7(c)* show the calculated values of K and $\langle w_{\max} \rangle$ versus Ra along with the best fits to the numerical data. Note that despite the qualitatively differences between 2D and the 3D flows found for $Ra > 47$, the maximum velocity of the mean flow coincides in both geometries. It is worthwhile to mention that the trend $\langle w_{\max} \rangle \sim Ra^{4/7}\kappa/h$ has been observed for a large range of Pr numbers in inclined heated from bellow cavities ($\alpha < 90°$) and that it has been also theoretically predicted (see [3]). Introducing the trends found for K and $\langle w' \rangle$ into equation (9) one obtains, $f_{\text{teor}} \sim Ra^{3/7}$. The fundamental frequency of the oscillation is shown in *figure 7(a)* versus the Rayleigh number. The best fit using the theoretical trend is $f_1 = 0.63\, Ra^{3/7}\nu/h^2$ and it is shown in dashed lines. As may be seen in *figure 7(a)* the qualitative agreement is excellent. Equation (9) gives $f_{\text{teor}} = 0.3\, Ra^{3/7}\nu/h^2$, so the order of magnitude of the theoretical approximation is consistent with the numerically obtained values of f_1. In conclusion, the dynamics of the fundamental oscillation is controlled by the longitudinal wave and the presence of the shear roll observed for $Ra \leqslant 156$ does not affect the temporal behaviour of the flow. Also, for the inclination considered ($\alpha = 80°$), the z-component of buoyancy does not alter the basic mechanism of the oscillations which is essentially the same that for horizontal cavities (see [14,10,11]).

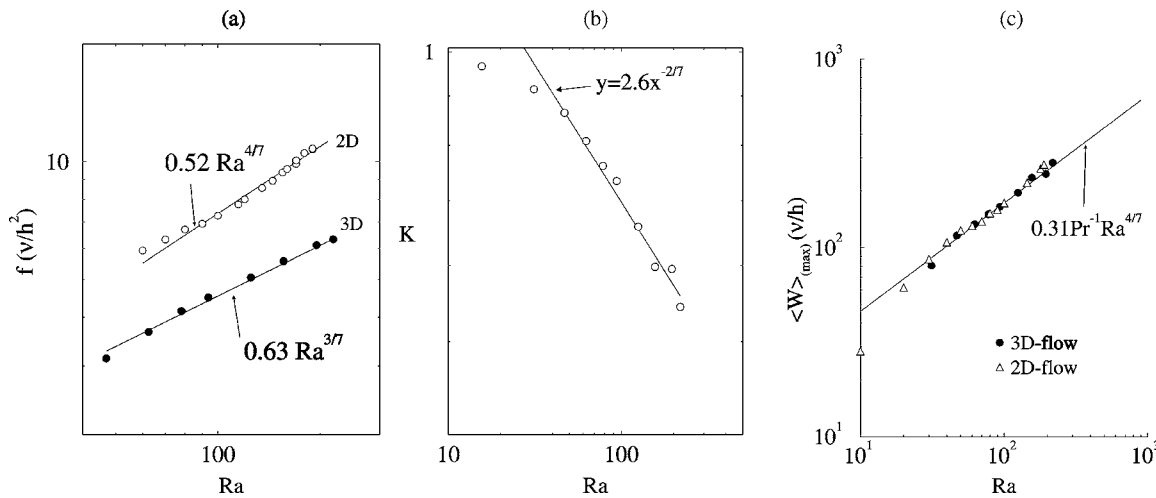

Figure 7. (a) Fundamental frequency of the 3D and the 2D flow versus *Ra*; (b) and (c) show respectively the mean temperature z-gradient at the core K and the maximum value of the mean z-velocity of the flow, $\langle W_{\max}\rangle$, versus *Ra*.

4.3. Transition to quasiperiodic flow, $Ra = 195$, and frequency locked state, $Ra = 219$

For $Ra \geqslant 195$ the time signals present a long period modulation. As shown in the power spectra of *figure 8(b)*, at $Ra = 195$, the frequency of the modulation is $f_2 = 1.135\nu/h^2$, nearly 6 times lower than the fundamental frequency, $f_1 = 6.10\nu/h^2$. The Poincare's sections of the phase orbits (see *figure 9(a)*) indicate that a transition to quasi-periodic flow has occurred. At a slightly greater value of the Rayleigh number, $Ra = 219$, both frequencies lock to $f_2 = 2f_1/11$, with $f_1 = 6.355\nu/h^2$. Components of frequency $f_2 = f_1/11$ are also seen in the power spectra obtained at $Ra = 219$ but as may be seen in *figure 8*, the dominant frequency of the modulation is $2f_1/11 = 1.155\nu/h^2$. *Figure 9* shows projection of the orbit in the phase-space and one of its Poincare's sections where a number of 11 spots are clearly visible.

In order to find the changes in the flow structure at the onset of the secondary frequency we put particular attention in the (x, z)-sections of the velocity field. Recall (see *table II*) that the flow has a unique transversal cell, at least for $20 \leqslant Ra \leqslant 156$ but at $Ra = 193$ two transversal co-rotating cells are clearly visible in the (x, z)-sections of the flow. The biperiodic flow consists on the three longitudinal rolls (related to the longitudinal wave that yields the fundamental period of the flow) and two transversal shear rolls that slightly oscillate along the z axis, with a period that corresponds to the secondary frequency. This bicellular pattern in the (x, z)-sections is directly observable from the velocity field when and where the intensity of the perturbative flow associated to the longitudinal wave is weaker. This is illustrated in *figures 5* and *6*. *Figure 5* shows a snapshot of the flow for $Ra = 193$ which was taken around at an instant of minimum intensity of the (x, y) perturbative flow. In this figure, the transversal bicellular flow may be directly observed in the (x, z) sections labeled by (1), (3) and (5) (the sections on the planes labeled by (3) and (5) have been magnified in *figures 5(d)* and *6(d)*). As seen in *figure 5(c)*, around these planes the perturbative z-velocity associated to the longitudinal wave reaches also its minimum intensity. *Figure 6* illustrates the flow at an instant separated from the snapshots in *figure 5* by roughly a quarter of the fundamental period. By the instant of *figure 6*, the intensity of the longitudinal rolls has increased to its maximum value and its presence apparently destroys the bicellular pattern, which is not directly visible at this stage of the fundamental cycle.

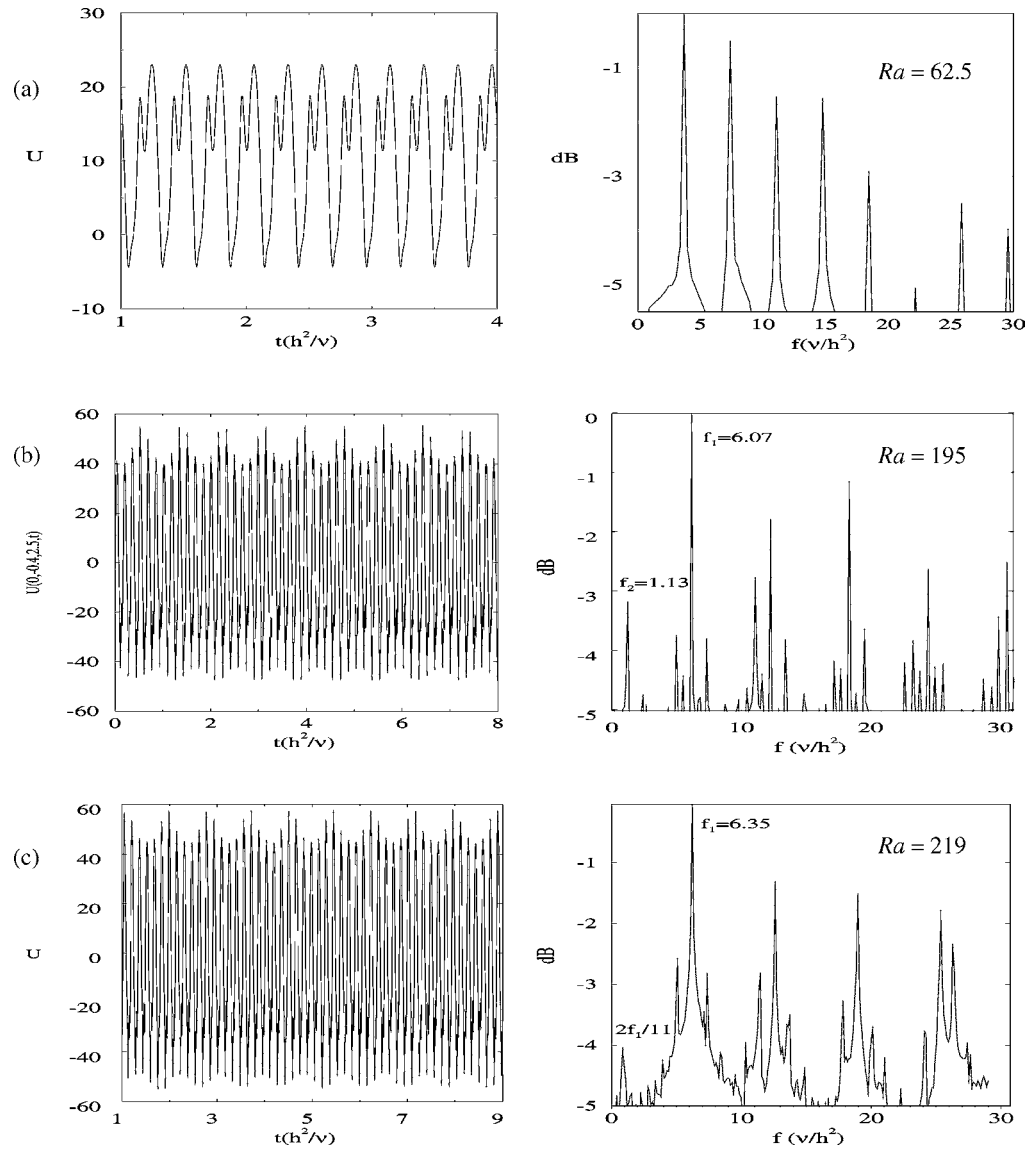

Figure 8. Time signal of the x-velocity obtained at $x/h = -0.09$, $y = -0.80A_y^{-1}$ and $z = 1.26A_z^{-1}$ (with $x \in [-1, 1]$, $y \in [-A_y^{-1}, A_y^{-1}]$ and $z \in [0, 2A_z^{-1}]$) and its power spectra for (a) $Ra = 62.5$, (b) $Ra = 195$ and (c) $Ra = 219$.

5. Conclusions

We have carried out numerical calculations of the convection of a low Prandtl number fluid ($Pr = 0.025$) in an inclined enclosure with dimensions $H \times D \times L = 1 \times 6 \times 4$ heated along its side of length L. For $\alpha = 90°$ the enclosure is in horizontal position and the linear stability analysis of the basic unicellular flow (see [12,15]) predicts that, as the Rayleigh number increases, the first instability to appear is the transversal stationary shear instability followed by a longitudinal oscillatory instability. Respectively, these instabilities are two and three-dimensional in nature. In this work, calculations have been made for a slightly smaller inclination, $\alpha = 80°$, at which the stability analysis [5] yields the same value of the critical Rayleigh number for both types of instabilities. The three-dimensional (3D) calculations were done by a finite volume method

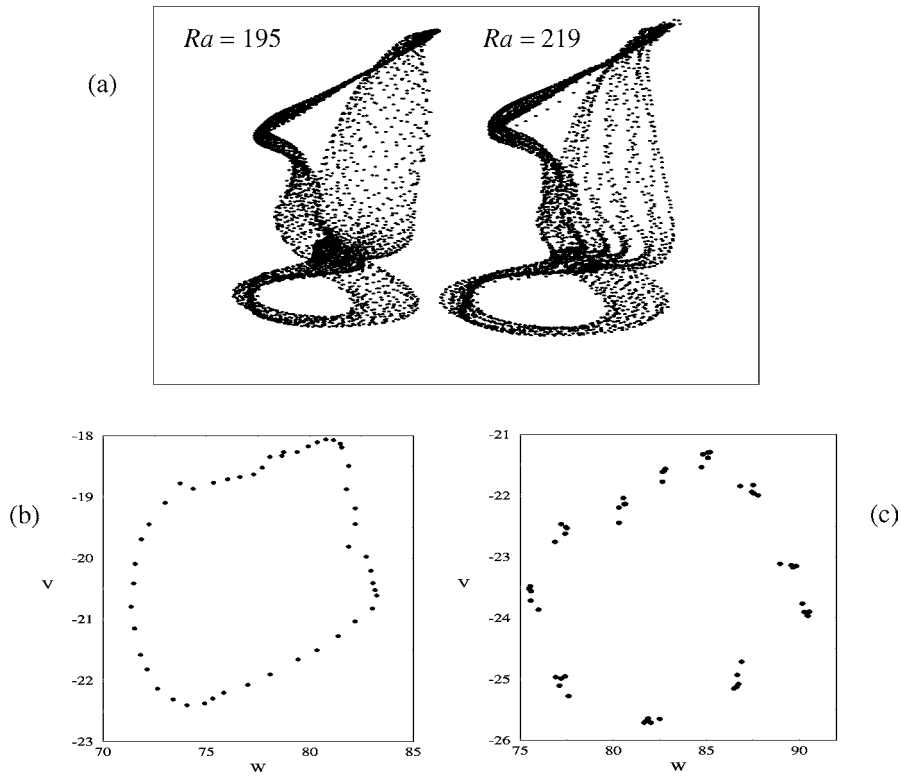

Figure 9. (a) Bidimensional projections of the torus in the phase-space and Poincare's sections obtained at $Ra = 193$; (b) in the quasiperiodic regime and at $Ra = 219$; (c) in a frequency locked state for which the the lowest frequency of the system is 11 times smaller that the fundamental one, f_1 (remark the 11 spots in (c)).

in a enclosure with $1 \times 6 \times 4$ and were compared with calculations in the two-dimensional 1×4 enclosure, made by a spectral method. For $Ra < 47$ the flow is bidimensional in nature and the 2D and 3D calculations gives similar results. In particular, at $Ra > 15$ a stationary shear roll begins to be formed in the center of the enclosure and its intensity gradually develops with Ra, according to an imperfect transition caused by the finite length ($L = 4H$) of the enclosure. The further transitions to time dependent flows are of different nature in the 2D and 3D situations. In the 2D enclosure, a Hopf bifurcation occurs at $55 < Ra \leqslant 60$ and the flow grows in complexity, loosing its centro-symmetry when a period-doubling bifurcation occurs at $90 < Ra \leqslant 100$. The 3D calculations show that the flow becomes three-dimensional at a lower value of Ra ($31.25 < Ra \leqslant 47$), due to the onset of the longitudinal oscillatory instability with three rolls along the width of the enclosure ($D = 6H$). The primary frequency grows as $f_1 \sim Ra^{3/7}\nu/h^2$; a trend which agrees with our theoretical relationship inspired by the analysis of Hart [10,11]. A secondary frequency appears at $Ra = 193$ and the 3D flow becomes quasiperiodic. Several transitions to biperiodic flow have been reported in previous studies on horizontal cavities and for different aspect ratios and Prandtl numbers [8,15,16,18]. A rather common hypothesis made in former experiments is that the secondary frequency could be due to a traveling wave formed by transversal rolls [15,16,18]. The present work gives the first numerical evidence on the connection between both facts. We have found that the onset of a quasiperiodic flow coincides with the formation of a bicellular transversal pattern that coexists with the longitudinal wave at least for $Ra \geqslant 193$ and whose associated frequency locks to $2/11$ times the fundamental one as Ra increases.

To conclude, it is worthwhile to mention that the inclined configuration enables a new dimension in the parameter space and therefore makes more feasible the study of several types of instabilities and their

corresponding interactions for suitable choices of the operating parameters [6,5]. This may be achieved using an experimental setup which may be simpler than the introduction of the Hartman number via a magnetic field [18,20].

Acknowledgements

We gratefully acknowledge J. García Sanz, I. Zuñiga and M.A. Rubio for fruitful discussions, and also, give thanks for the technical support given by Nicolas Coste and Eric Delboulbe at OptiFlow. P.B. acknowledges Action Intégrée PICASSO-99097. E.C.A. acknowledges support by DGESIC Projects BFM2000-0019 and PB98-0074. R.D.B. acknowledges grant support PB97-0077. Part of the numerical computations have been carried out on Cray YMP2E and CRAY C98 computers with support from scientific committees of IMT in Chateau-Gombert, Marseille, and from IDRIS CNRS, Paris.

References

[1] Hurle D.T.J., Jackman E., Johnson C.P., Convective temperature oscillations in molten gallium, J. Fluid. Mech. 64 (1974) 565.
[2] Markham B.L., Rosemberger F., Diffusive-convective vapor transport across horizontal and inclined rectangular enclosures, J. Cryst. Growth 67 (1984) 241.
[3] Delgado-Buscalioni R., Crespo del Arco E., Flow and heat transfer regimes in inclined differentially heated cavities, Int. J. Heat Mass Tran. 44 (2001) 1947–1962.
[4] Delgado-Buscalioni R., PhD thesis, Universidad de Educación a Distancia, Madrid, 1999.
[5] Delgado-Buscalioni R., Crespo del Arco E., Bontoux P., Ouazzani J., Convection and instabilities in differentially heated inclined shallow rectangular boxes, C. R. Acad. Sci. II B 36 (1998) 711–718.
[6] Delgado-Buscalioni R., Crespo del Arco E., Stability of thermally driven shear flows in long inclined cavities with end-to-end temperature gradient, Int. J. Heat Mass Tran. 42 (1999) 2811–2822.
[7] Braunsfurth M., Skeldon A.C., Juel A., Mullin T., Riley D.S., Free convection in liquid gallium, J. Fluid Mech. 342 (1997) 295–314.
[8] Braunsfurth M., Mullin T., An experimental study of oscillatory convection in liquid gallium, J. Fluid Mech. 327 (1996) 199–219.
[9] Henry D., Buffat M., Two and three dimensional numerical simulations of the transition to oscillatory convection in low-Prandtl-number fluids, J. Fluid Mech. 374 (1998) 145–171.
[10] Hart J.E., Stability of thin non-rotating Hadley circulations, J. Atmos. Sci. 29 (1972) 687.
[11] Hart J.E., A note on the stability of low-Prandtl-number Hadley circulations, J. Fluid Mech. 132 (1983) 271.
[12] Kuo H.P., Korpela S.A., Stability and finite amplitude natural convection in a shallow enclosure with insulated top and bottom and heated from a side, Phys. Fluids 31 (1) (1988) 33.
[13] Laure P., Study on convective in a rectangular enclosure with horizontal gradient of temperature, J. Méch. Théor. App. 6 (1987) 351–382.
[14] Gill A.E., A theory of thermal oscillations in liquid metals, J. Fluid. Mech. 65 (1974) 209.
[15] Hung M.C., Andereck C.D., Transitions in convection driven by a horizontal temperature gradient, Phys. Lett. A 132 (1988) 253–258.
[16] Pratte J.M., Hart J.E., Endwall driven, low Prandtl number convection in a shallow rectangular enclosure, J. Cryst. Growth 102 (1990) 54–68.
[17] Hart J.E., Pratte J.M., A laboratory study of oscillations in differentially heated layers of mercury, in: Roux B. (Ed.), Numerical Simulation of Oscillatory Convection in low-Pr Fluids, Notes on Numerical Fluid Mechanics, Vol. 27, Vieweg, 1990, pp. 338–343.
[18] Davoust L., Moreau R., Bolcato R., Control by a magnetic field of the instability of a Hadley circulation in a low-Prandtl-number fluid, Eur. J. Mech. B-Fluids 18 (1999) 621–634.
[19] Hung M.C., Andereck C.D., Subharmonic transitions in convection in a moderately shallow cavity, in: Roux B. (Ed.), Numerical Simulation of Oscillatory Convection in low-Pr Fluids, Notes on Numerical Fluid Mechanics, Vol. 27, Vieweg, 1990, pp. 338–343.
[20] McKell K.E., Broomhead D.S., Hones R., Hurle D.T.J., Torus Doubling in convecting molten gallium, Europhys. Lett. 12 (6) (1990) 513–518.
[21] Wang T., Korpela S.A., Secondary instabilities of convection in a shallow enclosure, J. Fluid Mech. 234 (1992) 147–170.
[22] Pulicani J.P., Crespo del Arco E., Randriampianina A., Bontoux P., Peyret R., Spectral simulations of oscillatory convection at low Prandtl number, Int. J. Numer. Meth. Fl. 10 (1990) 481–517.
[23] Skeldon A.C., Riley D.S., Cliffe K.A., Convection in a low Prandtl number fluid, J. Crystal Growth 162 (1996) 96–106.
[24] Afrid M., Zebib A., Oscillatory three dimensional convection in rectangular cavities and enclosures, Phys. Fluids A 8 (1990) 1318–1327.
[25] Vanel J.M., Peyret R., Bontoux P., A pseudospectral solution of vorticity-stream function equations using the influence matrix technique, in: Morton K.W., Baines M.J. (Eds.), Numerical Methods for Fluid Dynamics II, Clarendon Press, Oxford, 1986, pp. 463–475.
[26] Winters K.H., Oscillatory convection in liquid metals in a horizontal temperature gradient, Int. J. Numer. Meth. Eng. 25 (1989) 401–414.
[27] Gelfgat A.Yu., Tanasawa I., Numerical analysis of oscillatory instability of buoyancy convection with the galerkin spectral method, Numer. Heat Tr. A-Appl. 25 (1994) 627–648.
[28] Adaptive Research, CFD2000-Theoretical background, Pacific Sierra Corp., 1997.